This article was downloaded by:
On: *22 January 2011*
Access details: *Access Details: Free Access*
Publisher *Taylor & Francis*
Informa Ltd Registered in England and Wales Registered Number: 1072954 Registered office: Mortimer House, 37-41 Mortimer Street, London W1T 3JH, UK

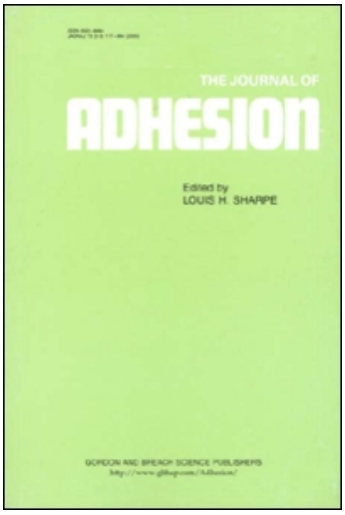

The Journal of Adhesion
Publication details, including instructions for authors and subscription information:
http://www.informaworld.com/smpp/title~content=t713453635

The Influence of Surface Properties on Carbon Fiber/Epoxy Matrix Interfacial Adhesion

H. Zhuang[a]; J. P. Wightman[a]
[a] Department of Chemistry, Center for Adhesive and Sealant Science, NSF Science & Technology Center, Virginia Polytechnic Institute & State University, Blacksburg, VA, USA

To cite this Article Zhuang, H. and Wightman, J. P.(1997) 'The Influence of Surface Properties on Carbon Fiber/Epoxy Matrix Interfacial Adhesion', The Journal of Adhesion, 62: 1, 213 — 245
To link to this Article: DOI: 10.1080/00218469708014570
URL: http://dx.doi.org/10.1080/00218469708014570

PLEASE SCROLL DOWN FOR ARTICLE

Full terms and conditions of use: http://www.informaworld.com/terms-and-conditions-of-access.pdf

This article may be used for research, teaching and private study purposes. Any substantial or systematic reproduction, re-distribution, re-selling, loan or sub-licensing, systematic supply or distribution in any form to anyone is expressly forbidden.

The publisher does not give any warranty express or implied or make any representation that the contents will be complete or accurate or up to date. The accuracy of any instructions, formulae and drug doses should be independently verified with primary sources. The publisher shall not be liable for any loss, actions, claims, proceedings, demand or costs or damages whatsoever or howsoever caused arising directly or indirectly in connection with or arising out of the use of this material.

J. Adhesion, 1997, Vol. 62, pp. 213–245
Reprints available directly from the publisher
Photocopying permitted by license only

© 1997 OPA (Overseas Publishers Association)
Amsterdam B.V. Published in The Netherlands under
license by Gordon and Breach Science Publishers
Printed in India

The Influence of Surface Properties on Carbon Fiber/Epoxy Matrix Interfacial Adhesion

H. ZHUANG and J. P. WIGHTMAN*

Department of Chemistry, Center for Adhesive and Sealant Science, NSF Science & Technology Center, Virginia Polytechnic Institute & State University, Blacksburg, VA 24061, USA

(Received 19 March 1996; In final form 3 December 1996)

Downloaded At: 11:17 22 January 2011

The mechanical performance of composite materials depends not only on the matrix and the reinforcing fiber, but also to a great extent on the fiber/matrix interfacial adhesion. The focus of this work was to study carbon fiber surface chemical and physical properties and their effects on fiber/matrix adhesion. Untreated, commercially-surface-treated, and oxygen-plasma-treated PAN-based carbon fibers were used. SEM was used to examine the fiber surface topography. XPS was used to determine fiber surface chemistry. A two-liquid tensiometric method was conducted to determine fiber surface energy and its dispersive and polar components. Carbon fibers with varying surface properties were incorporated into epoxy matrices. Single fiber fragmentation tests were carried out to evaluate the strength as well as the temperature and humidity effects on interfacial adhesion. Commercially-treated carbon fibers having a higher surface oxygen content and a higher surface energy clearly produced superior interfacial adhesion, relative to untreated fibers. An even greater level of adhesion was achieved with oxygen-plasma-treated fibers. Fiber surface roughness improved durability under elevated temperature and relative humidity conditions. The presence of sodium on the fiber surface dramatically decreased durability at high relative humidity.

Keywords: Composite; interfacial adhesion; carbon fiber; surface property; surface treatment; plasma treatment

*Corresponding author.

I. INTRODUCTION

A composite is an arrangement of reinforcing fibers in various configurations held together by a cohesive matrix. The fibers constitute the major load-bearing element of the composite and the role of the matrix is to both distribute the internal stress and protect the fibers from the environment. Factors which determine the mechanical performance of a composite are the strength and modulus of the fiber, the strength and chemical stability of the matrix resin, and the interfacial integrity between fiber and resin. The importance of the nature and degree of fiber/matrix interfacial adhesion on the mechanical performance of composites has been well established [1–3]. A weak interface tends to improve impact strength and fracture toughness of the composite by resisting cracks that would otherwise propagate through the matrix. A strong interface, on the other hand, insures effective stress transfer through the interface and improves off-axis strength. To achieve optimum performance, some compromise is needed between very strong and very weak interfacial adhesion.

In recent years, as composite material systems have become increasingly sophisticated to meet ever-increasing performance requirements, it has become more important to control the interaction between the reinforcing fibers and matrix materials. The major challenge here is the lack of fundamental understanding and knowledge about the reinforcement/matrix system which contributes to the establishment of the interface. It has been recognized that the state of the fiber surface substantially affects the quality of interfacial adhesion [4–6]. However, basic and specific correlation is still incomplete. The possible mechanisms by which the fiber surface parameters contribute to the constitution of the fiber/matrix interface include (i) the interfacial chemical and physical interactions caused by fiber surface functionality and surface energy, (ii) the mechanical interlocking due to fiber surface irregularity, and (iii) the interfacial wetting based on fiber surface energy.

It was the objective of this work to explore the effects of physical and chemical aspects of carbon fiber surfaces on the strength and durability of interfacial adhesion. Surface analytical techniques were utilized to obtain properties of untreated, commercially-surface-treated, and plasma-treated carbon fibers. The contributions of fiber surface characteristics to fiber/matrix adhesion were evaluated.

Downloaded At: 11:17 22 January 2011

II. EXPERIMENTAL

A. Materials

Carbon fibers used for this study were two untreated [AU-4 (Hercules), Panex 33 (U) (Zoltek)] and two commercially surface treated [AS-4 (Hercules), Panex 33 (S) (Zoltek)] polyacrylonitrile (PAN) based medium modulus carbon fibers. To study the effect of surface sodium on fiber/matrix adhesion, AS-4-Na fiber was prepared from AS-4 with electro-adsorbed surface sodium.

Amine cured epoxy systems were selected as matrix resins. A difunctional epoxy, diglycidyl ether of bisphenol-A (DGEBA), Epon® 828 (Shell), was cured with a stoichiometric amount of either an aromatic amine, mPDA (1,3-phenylene diamine) (Aldrich), or an aliphatic amine, Jeffamine® DU-700 (an amine-terminated urea condensate of polypropylene glycols) (Texaco). The cure schedule for both cases was two hours at 75°C and two hours at 125°C.

Downloaded At: 11:17 22 January 2011

B. Surface Analysis

1. Fiber Surface Topography by Scanning Electron Microscopy (SEM). An ISI SX-40 scanning electron microscope was used to examine the fiber surface topography. Carbon fibers were secured on a copper sample holder and sputter coated with gold for measurement. Secondary electron imaging was obtained usually at 15 kV accelerating voltage and 10 K magnification.

2. Fiber Surface Chemistry by X-ray Photoelectron Spectroscopy (XPS). The carbon fiber surface chemistry was determined by XPS using a Perkin-Elmer PHI 5400 X-ray photoelectron spectrometer with a nonmonochromatic Mg Kα X-ray source (1253.6 eV). All spectra were collected with the X-ray source operated at 15 kV and 400 W. The spot size was 1 mm × 3 mm and the take-off angle was 45°. The spectrometer was typically run at 10^{-8} torr. Data acquisition and analysis were performed using PHI software version 4.0. Binding energies were referenced to that of graphite carbon at 284.6 eV.

3. Fiber Surface Energy by Wetting Analysis. The two-liquid tensiometric technique developed by Schultz *et al.* [7] was used to access

carbon fiber surface energies and their dispersive and polar components. This method is based on the measurement of the wetting force of a single fiber by an immiscible two-liquid system of known surface free energies. The upper liquid was a series of non-polar *n*-alkanes and the bottom liquid was polar formamide. The relationship between surface energies and wetting force was given by,

$$\gamma_F - \gamma_H + F_2/p = 2(\gamma_S^d)^{1/2}[(\gamma_F^d)^{1/2} - (\gamma_H)^{1/2}] + 2(\gamma_F^P \gamma_S^P)^{1/2} \quad (1)$$

where $\gamma_F, \gamma_F^d, \gamma_F^P$ are the surface energy of formamide and its dispersive and polar components, respectively, γ_H is the surface energy of the hydrocarbon, γ_S^d, γ_S^P are the dispersive and polar components of carbon fiber surface energy, respectively, and F_2 is the wetting force at the fiber/hydrocarbon/formamide interface.

The tests were performed on a Cahn 322 dynamic contact angle analyzer. A single fiber was suspended from the arm of the microbalance while a precise elevator raised or lowered the test liquids at a speed of 20 μm/min to probe the fiber. Wetting force data were recorded at 1-second intervals for dynamic and static advancing immersion and receding emersion contact angles. The static advancing wetting force, that is, the plateau force reading when the advancing immersion was stopped, was used to calculate the carbon fiber surface energy. Five to six fibers were measured to get average values. A linear regression was made for experimentally-measured data $[\gamma_F - \gamma_H + F_2/p]$ *versus* $[(\gamma_F^d)^{1/2} - (\gamma_H)^{1/2}]$ and the slope and intercept provided a solution to the fiber surface energy terms γ_S^d and γ_S^P according to Equation (1). Fiber perimeters were determined using the wetting force by hexane which was assumed to wet the fibers completely.

4. Resin Surface Energy by Contact Angle Analysis and Fiber/Matrix Interfacial Work of Adhesion Calculation. The surface energy analysis of the cured epoxy resins was done using the method proposed by Owens and Wendt [8]. With this method, the values of the solid surface energy dispersive component, γ_S^d, and polar component, γ_S^P, can be determined from contact angles of two or more liquids against the solid. Water (double deionized), formamide, di-iodomethane and 1-bromonaphthalene were used as test liquids. The contact angle of each liquid against the resin surface was measured by the sessile drop method with a Rame-Hart 100-00 115 NRL contact angle goniometer.

Downloaded At: 11:17 22 January 2011

Drops of liquid, 5 microliters each, were carefully placed on the substrate using a microliter syringe. The contact angles on both sides of each drop were measured. Measurements from 6–10 drops were used to obtain an average value of the contact angle.

Epoxy surface energies were obtained by linear regression of contact angles plotted against liquid surface energies according to equation:

$$\frac{\gamma_L(1+\cos\theta)}{2\sqrt{\gamma_L^d}} = \sqrt{\gamma_S^d} + \sqrt{\gamma_S^p}\sqrt{\frac{\gamma_L^p}{\gamma_L^d}} \tag{2}$$

The interfacial reversible work of adhesion (W_{adh}) between the resin and carbon fiber defined by the Dupré equation as:

$$W_{adh} = \gamma_F + \gamma_R - \gamma_{F/R} \tag{3}$$

can be calculated from the resin and fiber surface energies by:

$$W_{adh} = W_{adh}^d + W_{adh}^p = 2(\gamma_F^d \gamma_R^d)^{1/2} + 2(\gamma_F^p \gamma_R^p)^{1/2} \tag{4}$$

where W_{adh}^d and W_{adh}^p are the reversible work of adhesion corresponding, respectively, to dispersive and polar interactions, γ_F^d and γ_F^p are the fiber dispersive and polar surface free energies, and, γ_R^d and γ_R^p are the resin dispersive and polar surface energies. Equation (4) is based on the semiempirical interfacial surface energy theory:

$$\gamma_{ab} = \gamma_a + \gamma_b - 2(\gamma_a^d \gamma_b^d)^{1/2} - 2(\gamma_a^p \gamma_b^p)^{1/2} \tag{5}$$

proposed by Fowkes [9].

C. Fiber/Matrix Adhesion Measurement

1. Single Fiber Fragmentation Technique. A review of publications on methods for measuring fiber/matrix adhesion led to selection of the single-fiber fragmentation test for this study because it is less sensitive to fiber local variations, straightforward in experimental procedure, and the results agrees well with other methods.

Downloaded At: 11:17 22 January 2011

With this method, the stress transfer capacity of the fiber/matrix interface is evaluated by a model single-fiber composite [10, 11]. The specimen is a dog-bone-shaped coupon which is composed of a single fiber embedded in a polymeric matrix. When the specimen is pulled in tension axially, the tensile load is transmitted to the fiber by the fiber/matrix interface. The tensile stress is much more concentrated in the fiber because of the large difference in moduli between the two materials. As a result, increasing stress will result in fiber fracture at some point. Further increase in stress will result in repetition of this process until a limiting size is reached which is defined as the critical fragment length, l_c. The interface of fragments with length shorter than the "critical length" can not transmit stress high enough to break the fiber. The capacity of the fiber/matrix interface to transfer stress can be reflected by this critical length in terms of the interfacial shear strength (IFSS), τ:

$$\tau = \frac{\sigma_f}{2}\frac{d}{l_c} \tag{6}$$

where d is the fiber diameter and σ_f is the fiber strength at the critical length. The critical length l_c can be conveniently measured to obtain the interfacial shear strength and, thus, the adhesion strength of fiber/matrix interface can be evaluated.

2. Carbon Fiber Diameter and Tensile Strength Determination. To obtain the interfacial shear strength, the carbon fiber diameter (d) and fiber tensile strength (σ_f) at the critical length is needed. Average fiber diameters calculated from 20 SEM photomicrographs of each fiber type were used for this purpose.

Since fiber strength is a function of fiber gauge length and direct measurement of σ_f at a gauge length of l_c is difficult, it is necessary to extrapolate fiber strengths measured at longer gauge lengths. In this study, the estimation of the fiber strength at l_c has been made using a linear logarithmic dependence of tensile strength on gauge length. This method of extrapolation was based on the weakest link theory of strength. A commonly used statistical model for strength is a two-parameter Weibull Equation [12].

$$F = 1 - \exp[-L(\sigma/\beta)^{\alpha}] \tag{7}$$

Downloaded At: 11:17 22 January 2011

where F is the probability of failure up to a stress level σ, L is the fiber gauge length, β is a scale parameter, and α is a shape parameter. The mean value, $\bar{\sigma}$, of the carbon fiber can be calculated from these parameters by using:

$$\bar{\sigma} = \beta L^{-1/\alpha}\Gamma\left(1 + \frac{1}{\alpha}\right) \tag{8}$$

Equation (8) shows that a plot of $\ln\bar{\sigma}$ *versus* $\ln L$ should yield a straight line.

Fiber tensile strengths were measured on single filaments at gauge lengths of 1, 12, 20, and 44 mm. Twenty data points were collected for each gauge length and the mean tensile strengths were obtained by the maximum likelihood approach of Equation (7). Fiber strengths at the critical length were calculated by extrapolation of the data from a linear regression in the log-log plot of fiber tensile strength *versus* gauge length down to the critical length which is usually fractions of a millimeter.

3. Preparation of Single Fiber Composite. Silicone rubber molds with dog-bone-shaped cavities were used for preparation of the single-fiber fragmentation samples. Single fibers were placed into the cavities and fixed by glass cloth electrical tape at ends. Epoxy resins were thoroughly degassed in vacuum and carefully poured into the cavities and filled to the level of the mold surface. The cure schedule was 75°C for 2 hours and then 125°C for another 2 hours. After cooling overnight in the oven, the specimens were demolded and stored in a desiccator until testing.

4. Interfacial Shear Strength by Single-Fiber Fragmentation Test. A single-fiber specimen was mounted in a hand-operated loading device which was placed on the stage in between of the polarizer and analyzer of a transmitting-light microscope. The orientation of the polarizer was perpendicular to the fiber and that of the analyzer parallel to the fiber. The sample was pulled in tension at a speed of 1 mm/min and the fiber-breaking process was observed. The pulling was stopped when no further breaks were observed. The fragment lengths were read with the aid of an eyepiece which was calibrated using a Weitzler stage micrometer.

Downloaded At: 11:17 22 January 2011

In practical measurement, instead of a single critical length, a distribution of fragments is observed due to fiber defects and heterogeneity. Therefore, a statistical analysis of the fragment data is needed. The two-parameter Weibull distribution was used for this purpose:

$$f(l) = \frac{\alpha}{\beta}\left(\frac{l}{\beta}\right)^{\alpha-1} \exp\left[-\left(\frac{l}{\beta}\right)^{\alpha}\right] \tag{9}$$

and the mean value determined by:

$$l_c = \beta\Gamma\left(\frac{\alpha+1}{\alpha}\right) \tag{10}$$

was used to calculate the interfacial shear strength from Equation (6). Data from six specimens were taken for each carbon fiber/matrix system.

Downloaded At: 11:17 22 January 2011

D. Interfacial Shear Strength (IFSS) After Humidity Exposure

It has been found that moisture and temperature are two environmental parameters that can have deleterious effects on the performance of advanced graphite-epoxy composites. The changes of IFSS with humidity exposure time were measured for the purpose of identifying the effects of surface properties on the humidity durability of interfacial adhesion.

The embedded single-fiber specimens of AU-4, AS-4, Panex 33(S) and AS-4-Na in the Epon 828-mPDA system were stored separately in desiccators which were (i) kept dry at 23°C, (ii) saturated with water vapor at 23°C 100%RH, (iii) kept dry at 75°C and, (iv) saturated with water vapor at 75°C 100%RH. Samples were removed from the desiccator periodically for measurement of interfacial shear strength.

E. Interfacial Shear Strength at Elevated Temperature

The changes of IFSS with temperature were determined by measuring IFSS at elevated temperature. The loading device and mounted single

fiber specimens were immersed in a thermostated silicone oil bath at set temperatures. After allowing 10 minutes to achieve steady state, the temperature was recorded and the sample was pulled in tension to the desired elongation at a rate 1mm/min. The specimen was unloaded immediately after the device was retrieved from the hot bath. The sample was examined under a polarized transmitting-light microscope and break lengths were read with the aid of birefringence.

F. Matrix Resin Structure Analysis

Cured epoxy resin powder was taken from the surface of the original, the sodium/humidity, and the sodium/humidity/temperature exposed dog-bone samples. Pellets were prepared by pressing a mixture of KBr and resin powder. Transmission IR spectra were obtained using a Nicolet 5DXB Fourier transform infrared spectrometer with a resolution of 2 cm^{-1}. The spectrometer was purged with dry nitrogen prior to and during the measurement.

Downloaded At: 11:17 22 January 2011

G. Plasma Treatment of Carbon Fibers

AU-4 and Panex 33(U) fibers were oxygen plasma treated to investigate the effects of plasma on carbon fiber surface characteristics and interfacial adhesion. Plasma treatments were carried out in a March Instruments Plasmod unit. The unit was operated at 13.56 MHz frequency, 50 watts power and 1 torr of pressure. Prior to activating the RF field, the plasma chamber was pumped down to 1 torr and filled to 400 torr with oxygen twice to minimize the residual air content.

Treated carbon fibers for interfacial shear strength measurements were immersed with mixed resin and hardener immediately after removal from the plasma chamber. Fibers for surface analyses were stored in a desiccator. Surface chemistry analysis by XPS was carried out within 30 minutes, surface energy analysis by the two-liquid dynamic contact angle method within 5 days, and surface morphology by SEM within 10 days.

III. RESULTS AND DISCUSSION

A. Carbon Fiber Surface Topography

Scanning electron microscopy provides a direct view of the fiber surface topography. The SEM photomicrographs of the fibers used in this study at magnification of 10,000 × are shown in Figure 1. The Hercules AU-4 and AS-4 fibers are relatively featureless and smooth, whereas the Panex 33(U) and Panex 33(S) fibers showed a rather rough surface topography.

The topographic changes in the carbon fiber surface caused by oxygen plasma treatment are shown in the SEM photomicrographs in Figure 2. Some evidence of etching and pitting can be seen in plasma-treated AU-4 fiber but that is not so evident in Panex 33 (U) fiber at the resolution of the SEM.

Downloaded At: 11:17 22 January 2011

B. Carbon Fiber Surface Chemistry

Qualitative analysis of as-received and oxygen-plasma-treated carbon fiber surfaces in the XPS survey scan mode identified the existence of carbon, oxygen, nitrogen, and sodium. Quantitative analysis results from the multiplex scan peak areas and corresponding photoelectron cross section of the elements are listed in Table I. Carbon is the primary element; oxygen is attributed to oxidation of carbon fiber surface and adsorbed materials; nitrogen is attributed to the PAN source and adsorbed materials; and sodium is attributed to the alkyl sodium thiocyanate added to the spinning precursor.

Compared with AU-4 and Panex 33(U), AS-4 and Panex 33(S) both have a higher level of surface oxygen produced by commercial surface pretreatment. Angle-dependent XPS results showed that oxygen is more concentrated on the very top surface.

A considerable amount of sodium was observed on the Panex 33(S) fiber which was taken from an early production run. It has been assumed that the presence of sodium on a carbon fiber surface is harmful because it could induce both degradation of the matrix resin and oxidization of the carbon fiber. To study the effect of surface sodium and isolate this effect from other variations, AS-4-Na fiber was

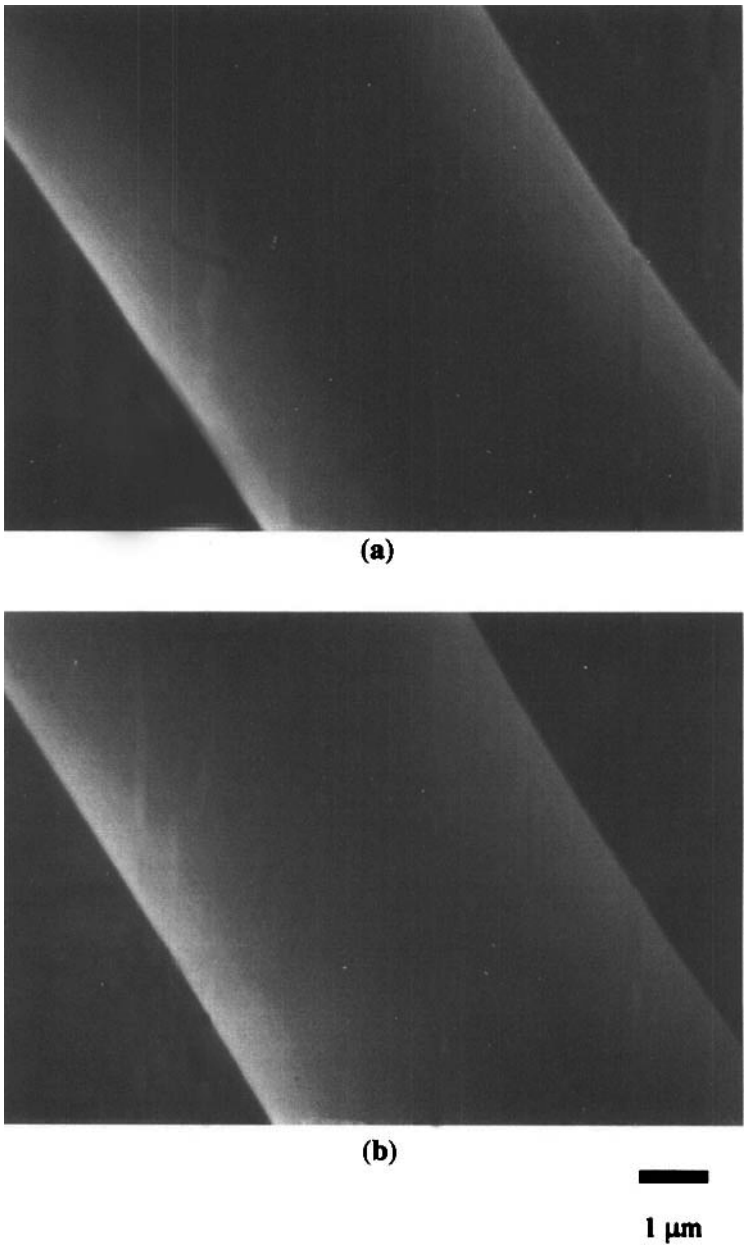

FIGURE 1 SEM photomicrographs of carbon fibers. (a) Hercules AU-4, (b) Hercules AS-4, (c) Zoltek Panex 33 (U), and (d) Zoltek Panex 33 (S).

Downloaded At: 11:17 22 January 2011

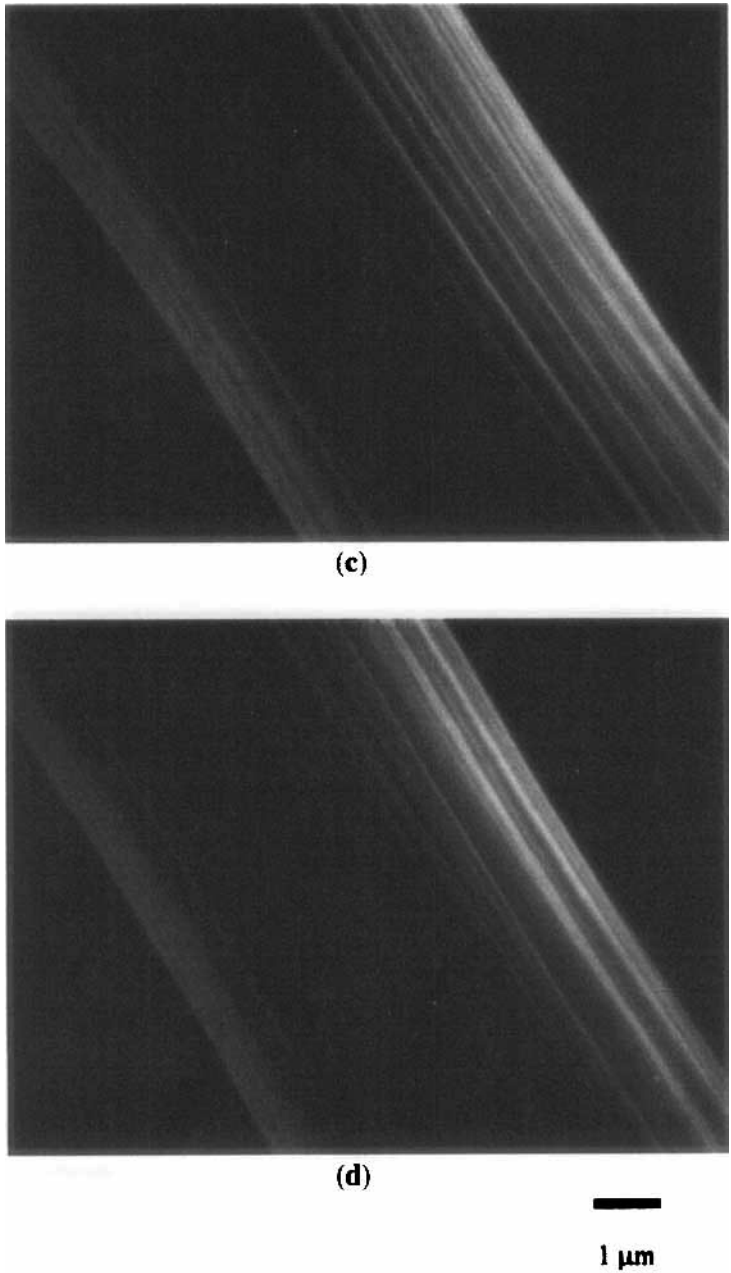

FIGURE 1 (Continued).

Downloaded At: 11:17 22 January 2011

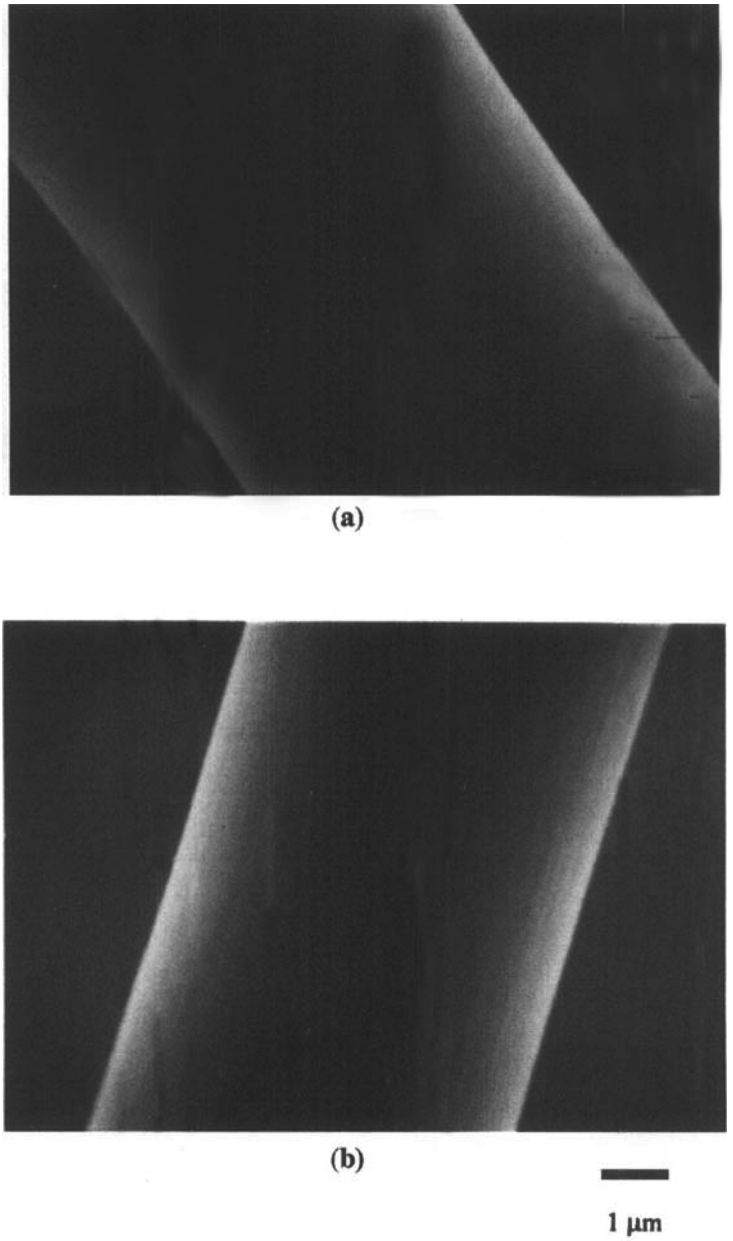

FIGURE 2 SEM photomicrographs of carbon fibers after exposure to an oxygen plasma. (a) AU-4 original, and (b) AU-4 90 sec. plasma, (c) Panex 33 (U) original, and (d) Panex 33 (U) 90 sec. plasma.

Downloaded At: 11:17 22 January 2011

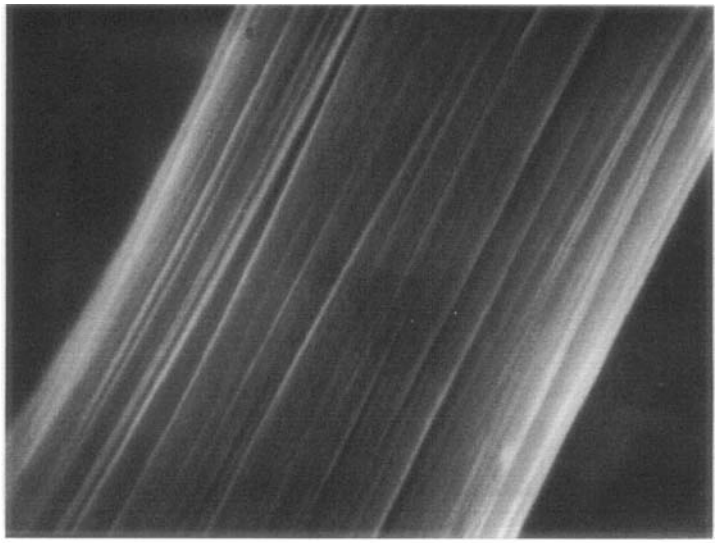

(c)

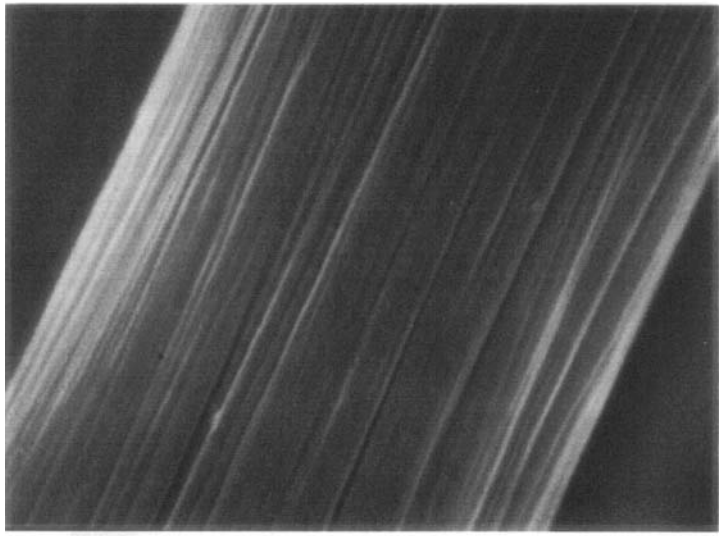

(d)

1 μm

FIGURE 2 (Continued).

Downloaded At: 11:17 22 January 2011

TABLE I XPS surface composition of carbon fibers

Fiber	*Surface Composition (atom%)*			
	Carbon	*Oxygen*	*Nitrogen*	*Sodium*
AU-4	94 ± 1.2	3.1 ± 0.9	2.5 ± 0.2	0.04 ± 0.03
AS-4	85 ± 1.3	12 ± 0.7	3.6 ± 0.3	0.34 ± 0.15
Panex 33 (U)	93 ± 1.2	4.7 ± 1.0	1.8 ± 0.4	0.43 ± 0.10
Panex 33 (S)	80 ± 1.5	9.1 ± 1.2	7.6 ± 0.4	3.0 ± 0.5
AS-4-Na	85 ± 0.9	10 ± 0.5	3.2 ± 0.2	2.3 ± 0.4

prepared from AS-4 fiber. A surface sodium concentration of 2.3% was determined by XPS.

XPS photoelectron peak shape analysis by curve fitting gives another level of surface chemistry information about chemical states. For instance, the carbon 1s graphite peak at 284.6 eV exhibits an asymmetric tailing toward high binding energy. This tail is caused partly by the main graphite peak's intrinsic asymmetry and also by the chemical shift of photoelectron peaks associated with functionalized carbons. Ideally, the type of functionality can be determined by the extent of this chemical shift.

The fiber surface carbon 1s photopeaks were curve fitted into six peaks as shown in Figure 3. Table II lists the peak positions, area percentages and peak assignments. The peak assignments were based on published works [13–16]. Curve fitting results indicate that the fiber surface carbon was functionalized by oxygen and nitrogen in several bonding states. Commercial fiber surface pretreatment increased fiber surface oxygen in all bonding states.

It was determined by XPS surface analysis that significant changes in the surface composition of as-received (untreated) carbon fiber occurred during oxygen plasma treatment. As shown in Figures 4 and 5, exposure to oxygen plasma significantly increased the surface oxygen content and slightly increased the nitrogen and sodium contents of both AU-4 and Panex 33(U) fibers. The plasma species reacted with the carbon fiber quickly and saturation was reached in about 15 seconds. Saturation is the limit of carbon fiber surface functionalization corresponding to a steady state established where the rate of functionalization is equal to the rate of plasma erosion.

Downloaded At: 11:17 22 January 2011

The curve fit carbon 1s photoelectron peaks of carbon fibers before and after oxygen plasma treatment are shown in Figure 6. Table III lists the peak positions and area percentages. The carbon peak curve

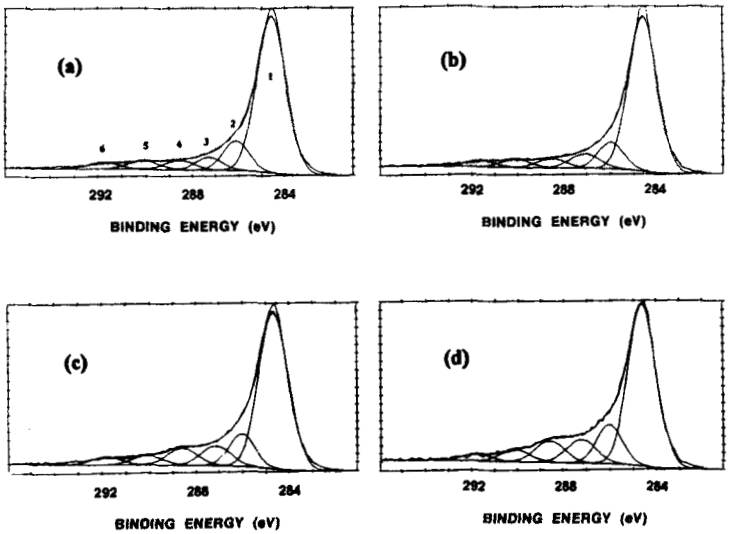

FIGURE 3 Curve fit carbon 1s XPS photoelectron peaks of (a) AU-4, (b) AS-4, (c) Panex 33 (U), and (d) Panex 33 (S) carbon fibers.

TABLE II Carbon 1s photopeak curve fit results of carbon fibers

Fiber	*Binding Energy (eV)**					
	284.6	*285.9*	*287.2*	*288.6*	*290.0*	*291.7*
AU-4	70.2	11.7	7.0	4.2	3.8	3.1
AS-4	64.7	12.4	8.1	7.0	4.4	3.4
Panex 33 (U)	71.4	11.2	6.7	4.2	3.7	2.8
Panex 33 (S)	61.1	13.6	9.4	8.5	4.7	2.7
Assignment	C—C C—H (graphite, aromatics, aliphatics)	C—OH C—O—C C—N C=N C≡CN	C=O N—C=O	O=C—OH O=C—OR	O—C—O O=C—O⁻ O=C—O	plasmon
Peak No.	1	2	3	4	5	6

*Gaussian function curve fit. Uncertainty in peak position is ±0.1 eV, FWHM are 1.4 ± 1 eV.

Downloaded At: 11:17 22 January 2011

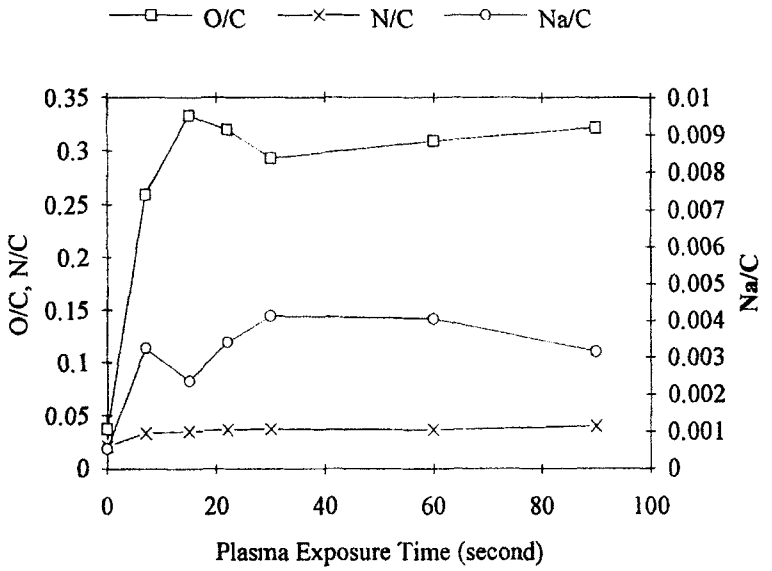

FIGURE 4 AU-4 carbon fiber surface composition as a function of oxygen plasma treatment time.

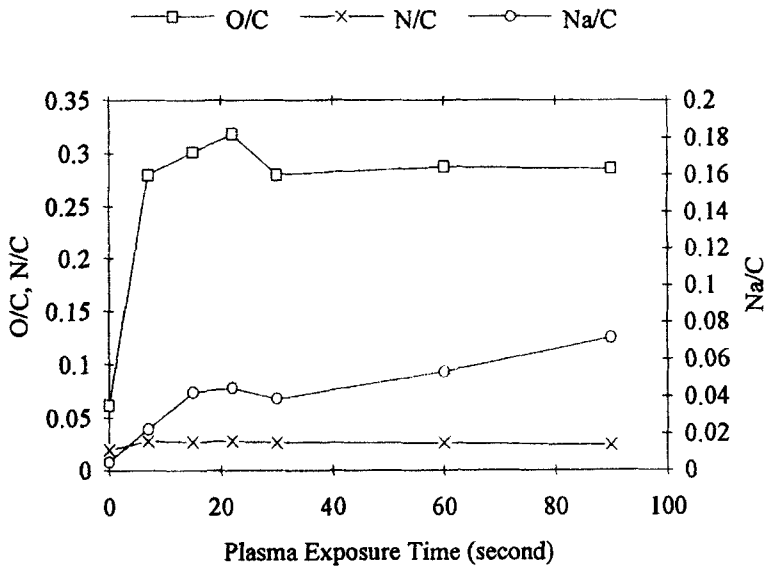

FIGURE 5 Panex 33 (U) carbon fiber surface composition as a function of oxygen plasma treatment time.

Downloaded At: 11:17 22 January 2011

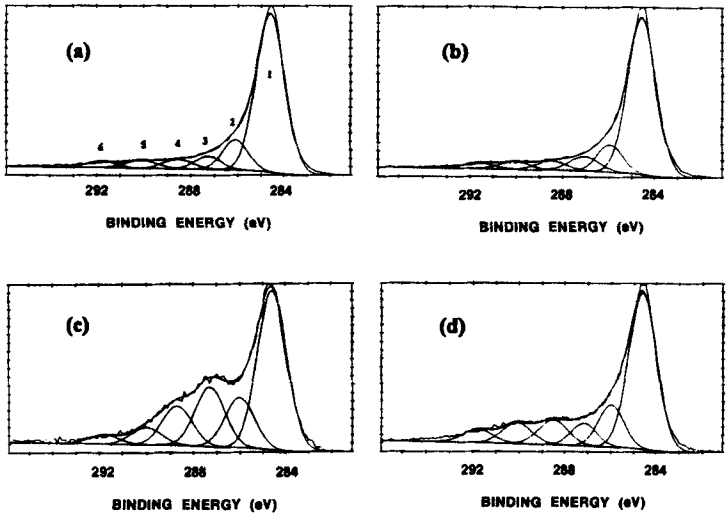

FIGURE 6 Curve fit carbon 1s XPS photoelectron peaks of (a) AU-4 original, (b) Panex 33 (U) original, (c) 90 sec. oxygen-plasma-treated AU-4, and (d) 90 sec. oxygen-plasma-treated Panex 33 (U) fibers.

Downloaded At: 11:17 22 January 2011

fit results indicate that exposure to an oxygen plasma increased the amount of oxygen-functionalized carbon groups on the fiber surface. The peak assignments are the same as given in Table II.

C. Carbon Fiber Surface Energy

Values of the polar, dispersive, and total surface energies of carbon fibers obtained by the two-liquid wetting analysis are listed in Table IV. Compared with untreated fibers, the two commercially-surface-pretreated fibers (AS-4 and Panex 33(S)) exhibited higher surface energies principally due to the polar component. This result paralleled the higher surface oxygen levels for these two fibers determined by XPS analysis (see Tab. I).

Paralleling the incorporation of surface functional groups on the fiber, the polar surface energy increased significantly by oxygen plasma treatment. The change of the fiber polar surface energy with plasma treatment time is shown in Figure 7. Saturation was reached quickly in about 15 seconds. The values were slightly higher for Panex 33 (U) compared with the AU-4 fibers.

TABLE III Carbon 1s photopeak curve fit results of oxygen-plasma-treated carbon fibers

Fiber	*Binding Energy (eV)**					
	284.6	*285.9*	*287.2*	*288.6*	*290.0*	*291.7*
AU-4, original	70.2	11.7	7.0	4.2	3.8	3.1
AU-4, 7 sec. O_2 plasma	54.2	15.8	13.9	8.6	4.5	3.0
AU-4, 15 sec. O_2 plasma	48.4	14.4	18.1	11.9	4.5	2.7
AU-4, 30 sec. O_2 plasma	53.0	14.2	14.9	10.4	4.8	2.7
AU-4, 90 sec. O_2 plasma	46.6	14.5	18.9	11.9	5.3	2.8
Panex 33 (U), original	71.4	11.2	6.7	4.2	3.7	2.8
Panex 33 (U), 7 sec. O_2 plasma	60.5	11.6	10.6	8.2	5.3	3.8
Panex 33 (U), 15 sec. O_2 plasma	62.0	12.3	10.6	7.6	4.3	3.2
Panex 33 (U), 30 sec. O_2 plasma	59.8	13.5	8.9	7.9	5.9	4.0
Panex 33 (U), 90 sec. O_2 plasma	57.3	13.3	7.1	9.4	7.9	5.0
Peak No.	1	2	3	4	5	6

*Gaussian function curve fit, uncertainty in peak position is ± 0.1 eV, FWHM are 1.4 ± 0.1 eV.

TABLE IV Carbon fiber surface energies (in mJ/m^2)

Fiber	γ_s^d	γ_s^p	γ_s^{Total}
AU-4	46.4	6.86	53.2
AS-4	56.9	16.3	73.2
Panex 33 (U)	44.5	7.48	51.0
Panex 33 (S)	50.9	19.5	70.4

Downloaded At: 11:17 22 January 2011

D. Fiber/Matrix Adhesion

The single-fiber fragmentation test does not yield a single l_c but a distribution because of the fiber surface flaws. Figure 8 shows some typical Weibull plots of fragment lengths obtained from the fragmentation tests. The l_c values used in the IFSS calculations were taken as the statistical mean of the two-parameter Weibull distribution.

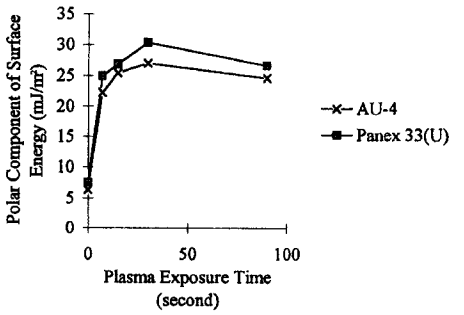

FIGURE 7 Polar component of fiber surface energy as a function of oxygen plasma treatment time.

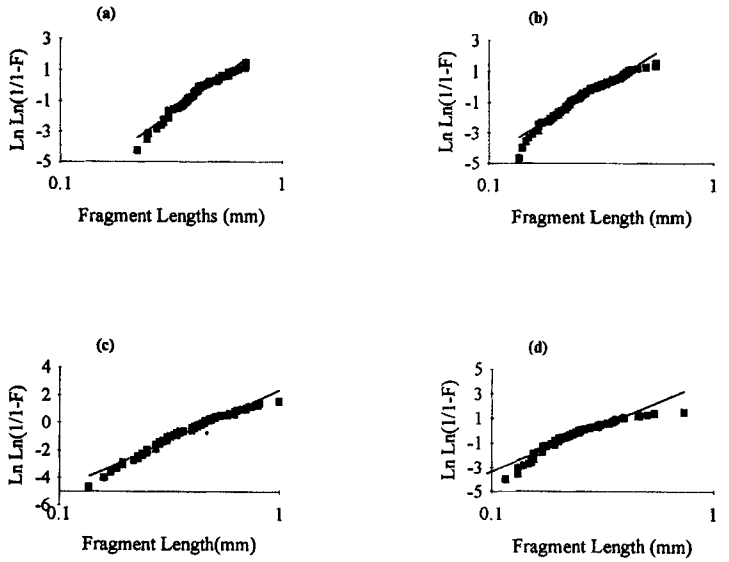

FIGURE 8 Weibull plots of fragment lengths by single fiber fragmentation tests for the fiber/Epon 828-mPDA system. (a) AU-4 fiber, (b) AS-4 fiber, (c) Panex 33 (U) fiber, and (d) Panex 33(S) fiber.

Downloaded At: 11:17 22 January 2011

Surface-treated AS-4 and Panex 33 (S) fibers gave substantially higher levels of interfacial adhesion with both expoxy matrices compared with untreated fibers based on calculated interfacial shear strengths. The improved interfacial adhesion may result from the increased fiber surface oxygen content, increased polar component and, therefore, total fiber surface energy by surface treatment. Figures 9 and 10 show the direct correlation between interfacial shear strength and fiber surface O/C ratio and fiber surface energy. The error bars represent the standard deviation of the mean value for each of the six samples tested. Another possible effect is that surface treatment may remove a weakly-bound layer from the original fiber surface leading to a mechanically sound surface to which the resin can form a good bond as suggested by Drzal *et al.* [17].

Surface roughness is another factor possibly affecting interfacial adhesion. Two types of surface topography were available in this study. The Panex 33(U) and Panex 33(S) fibers had rough, striated surfaces whereas the AU-4 and AS-4 had rather smooth surfaces. A general model by Nardin *et al.* [18] proposed that a linear relationship should exist between the interfacial shear strength (τ) and the

Downloaded At: 11:17 22 January 2011

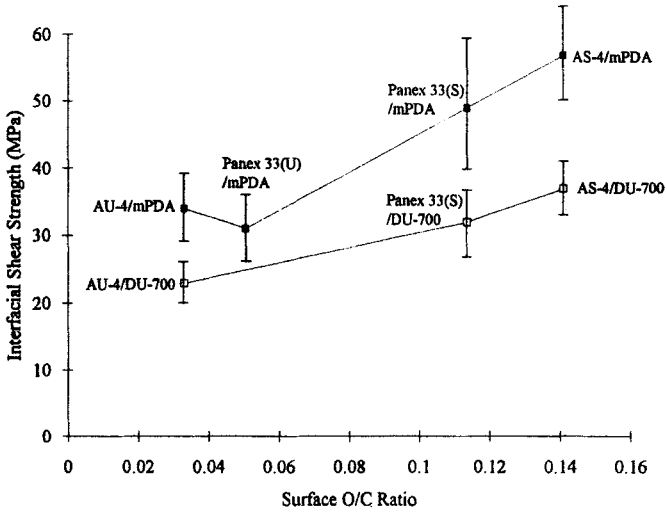

FIGURE 9 Relationship between interfacial shear strength and fiber surface oxygen content.

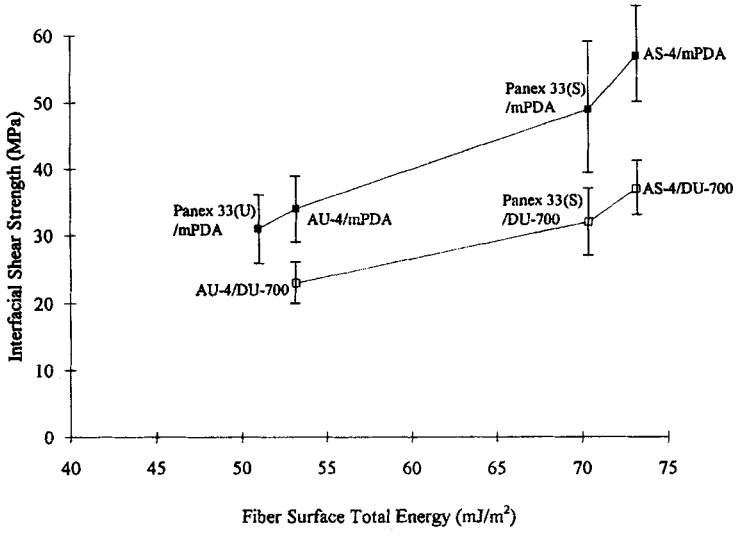

FIGURE 10 Relationship between interfacial shear strength and fiber surface energy.

Downloaded At: 11:17 22 January 2011

reversible energy of adhesion (W_0):

$$\tau = \left(\frac{E_m}{E_f}\right)^{1/2} \frac{W_0}{\lambda} \tag{11}$$

where E_m and E_f are the moduli of matrix and fiber, respectively, and λ is a constant corresponding to the distance between atoms undergoing physical interaction. Figure 11 shows the relationship between the interfacial work of adhesion and interfacial shear strength. For both systems, Panex fibers gave a lower level of adhesion instead of a higher level as expected for a rough surface morphology by a mechanical interlocking type mechanism. This discrepancy was attributed to incomplete filling of valleys of the fiber surface striations by the matrix resin leading to a reduction of interfacial area. When the resin came in contact with the striated fiber surface, small amounts of residual air could have been sealed in the bottom of the valleys and was not eliminated during the curing process. Figure 12 shows the SEM photomicrograph of the cross section of the Panex 33(S)/Epon 828-DU-700 single fiber composite.

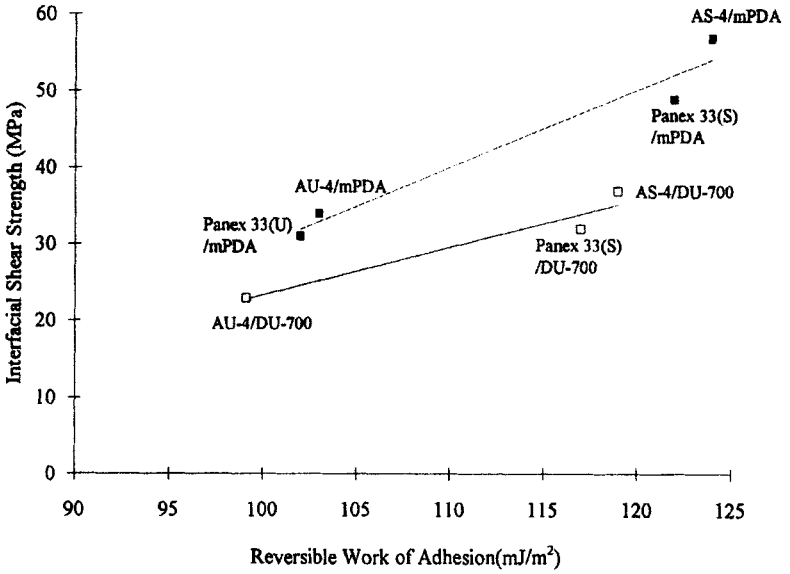

FIGURE 11 Relationship between the reversible work of adhesion and interfacial shear strength.

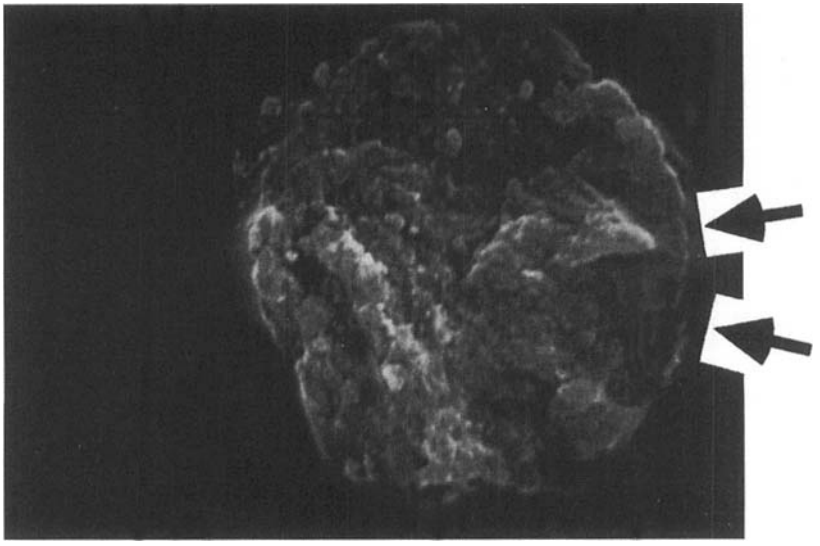

FIGURE 12 SEM photomicrograph of the Panex 33 (S)/Epon 828-DU700 interface.

Downloaded At: 11:17 22 January 2011

Some void areas at the bottom of the striations between fiber and matrix are visible.

E. Effect of Temperature

The influence of temperature on the interfacial shear strength (IFSS) measured by the single fiber fragmentation test is illustrated in Figures 13 and 14. The glass transition temperatures measured by DSC were 144°C for mPDA-cured Epon 828 and 19°C for Jeffamine DU-700-cured Epon 828.

In the fiber/Epon 828-mPDA system, in which all temperatures were below Tg, the IFSS generally decreased with increasing temperature. The decrease of matrix modulus with increasing temperature was one cause for the IFSS reduction. The predictions of the effect of matrix modulus on interfacial adhesion by researchers based on varying assumptions end up with a similar expression [18]:

$$\frac{l_c}{d} = C\sqrt{\frac{E_f}{G_m}} \tag{12}$$

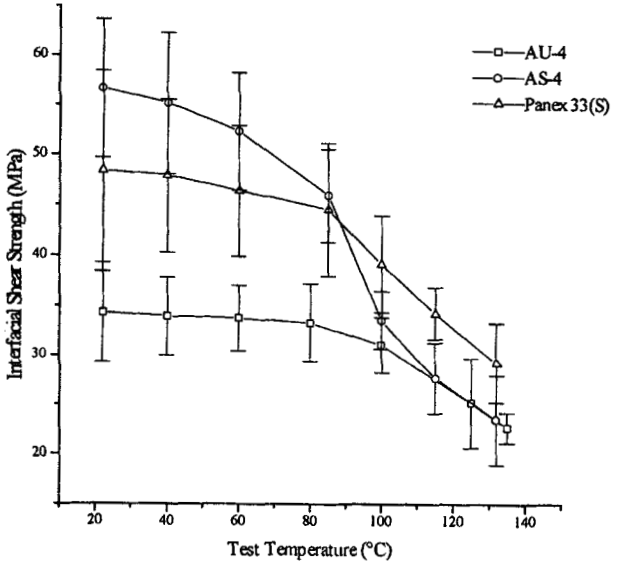

FIGURE 13 Temperature dependence of interfacial shear strength for AU-4, AS-4 and Panex 33 (S) fibers in Epon 828/mPDA.

Downloaded At: 11:17 22 January 2011

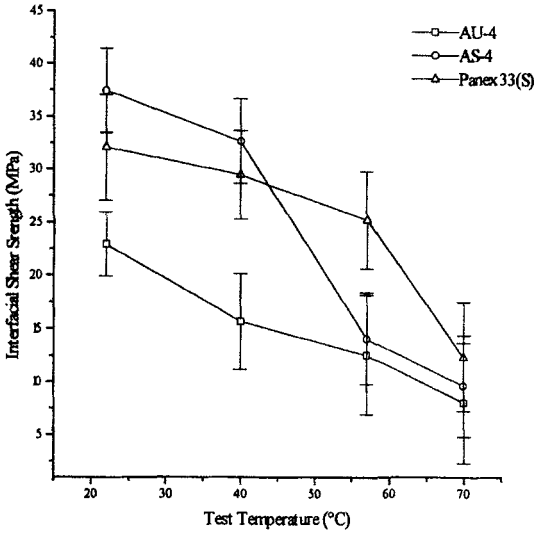

FIGURE 14 Temperature dependence of interfacial shear strength for AU-4, AS-4 and Panex 33 (S) fibers in Epon 828/Jeffamine DU-700.

Downloaded At: 11:17 22 January 2011

where l_c is the critical fragment, d is the fiber diameter, C is a proportionality constant, and E_f and G_m are the Young's modulus of the fiber and the shear modulus of the matrix, respectively.

A dramatic decrease in IFSS, especially in the AS-4 fiber system (see Fig.13), was observed at temperatures about 80°C which is much lower than the glass transition temperature of the bulk polymer. After this major decrease, the IFSS of the surface-treated AS-4 fiber system decreased to essentially the same level as that of the untreated AU-4 fiber system. Two reasons were suggested to account for this effect. (i) At low temperature, the interfacial strength was controlled by interfacial interactions and systems with different surface properties lead to different levels of adhesion. However, there exists an interphase zone of lower glass transition temperature and lower modulus than the bulk matrix as suggested by other authors [19–21]. When the temperature was increased (even though still lower than the bulk matrix Tg), the properties of this interface zone decreased such that the interphase matrix became the weakest linkage in the system. The interface strength was then matrix-controlled which is the same for all the

fibers. (ii) Treated fibers, with higher surface energy and more surface functionalization, established more atomic/molecular interactions with the matrix resin at low temperature. With increasing temperature, thermal motion increased and kinetic energy ($3/2\,RT$) overcame the hydrogen and secondary bonding energies so that these forces no longer contributed as much to the interfacial adhesion as at low temperature. The fact that AS-4 and AU-4 fell to the same adhesion level after 100°C suggested that surface-treated As-4 fiber had not formed significantly more chemical bonding with the matrix resin because much higher temperature would be needed to break chemical bonds.

Although the Panex 33(S) fiber did not give superior initial interfacial adhesion, this system maintained a higher IFSS over a wider temperature range than AS-4. This fact can be attributed to the greater degree of surface roughness of Panex 33(S) fiber compared with the AS-4 fiber. The interfacial interactions predominated at low temperature whereas mechanical interlocking caused by surface roughness enhanced the IFSS when interfacial interactions were diminished at high temperature.

In the Jeffamine DU-700-cured Epon 828 systems (see Fig. 14), in which all temperatures were all above Tg, similar tends were found. IFSS decreased with temperature. The AS-4 and AU-4 systems fell to a similar level of IFSS at high temperature. Panex 33(S) gave higher IFSS over a wider temperature region than the AS-4 fiber.

Downloaded At: 11:17 22 January 2011

F. Effect of Humidity

The effect of humidity on the durability of the fiber/matrix interface was studied by measuring the interfacial shear strength after specimens were exposed to humidity environments for a period of time. For the effect of humidity to be tested in a reasonable time, the fiber was placed near the surface of the specimen. The depth of the fiber in the matrix was measured by a micrometer, with the aid of a microscope, as 0.2 mm from the sample surface.

The IFSS values for the Epon 828/mPDA samples stored at dry conditions at 23°C and 75°C are shown in Figures 15 and 16, respectively. The IFSS of samples stored under dry conditions stayed essentially constant even at the storage temperature of 75°C. Figures 17 and 18

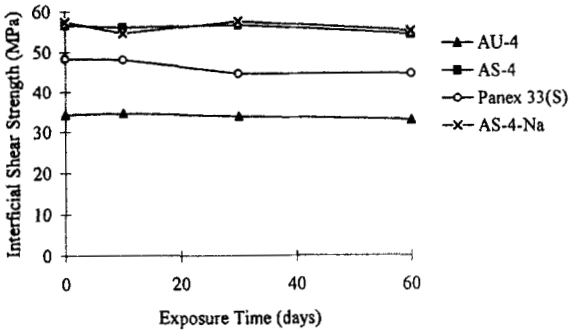

FIGURE 15 The influence of exposure time on interfacial shear strength in fiber/Epon 828-mPDA system at 23°C 0% RH.

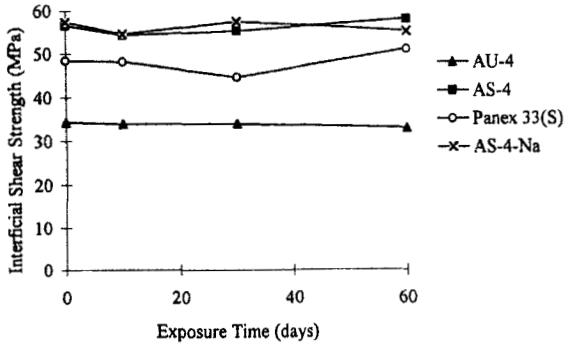

FIGURE 16 The influence of exposure time on interfacial shear strength in fiber/Epon 828-mPDA system at 75°C 0% RH.

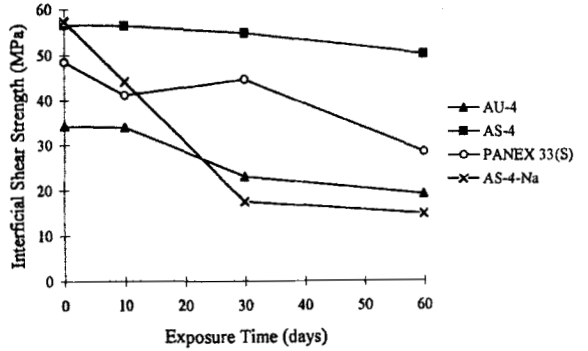

FIGURE 17 The influence of exposure time on interfacial shear strength in fiber/Epon 828-mPDA system at 23°C 100% RH.

Downloaded At: 11:17 22 January 2011

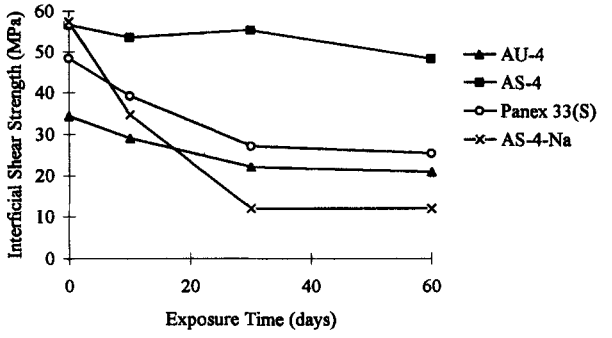

FIGURE 18 The influence of exposure time on interfacial shear strength in fiber/Epon 828-mPDA system at 75°C 100% RH.

Downloaded At: 11:17 22 January 2011

show the interfacial shear strength changes when single fiber specimens were exposed in humid atmospheres. The IFSS of samples exposed to either 23°C or 75°C water-vapor-saturated environments decreased with exposure time indicating the degradation of interfacial adhesion by moisture.

The deleterious effect of moisture on interfacial adhesion has been studied by other authors [22–25] and was attributed mainly to matrix plasticization and a decrease in glass transition temperature by moisture absorption. Epoxy resin systems are especially susceptible to moisture attack because of the hydrophilic nature of the resins.

AS-4-Na fiber initially gave the same IFSS as AS-4 fiber (see Figs. 17 and 18) indicating that surface sodium did not affect the initial interfacial shear strength. However, upon exposure to humidity, the IFSS of the AS-4-Na system decreased much more dramatically than the other fiber systems documenting the fact that sodium contamination on a carbon fiber surface has a very deleterious effect on fiber/matrix durability.

The effects of sodium on the hydrolysis degradation of the epoxy resin were studied by FTIR analysis of resin samples exposed to humidity and aqueous Na_2CO_3 solutions. The amine cured epoxy network is usually quite stable to aqueous and alkaline aqueous media. If any degradation occurs, it is expected that elimination of —OH and formation of olefin and, even further, cleavage of C—N bonds and formation of aldehyde will occur. Neither olefin nor aldehyde were

present in the original resin and, thus, any degradation could be easily detected in FTIR spectra. The transmission FTIR spectra of samples exposed to humidity and aqueous Na_2CO_3 at 23°C and 75°C are shown in Figure 19. The olefin bond vibration at 1648 cm^{-1} and aldehyde bond vibration at 1700 cm^{-1} were only slightly evident (see Fig. 19e) under the most severe condition, that is, when dipped in 10% Na_2CO_3 solution at 75°C for 30 days. These results support the conclusion that no significant resin degradation under test conditions.

Therefore, it is concluded that the hygroscopic nature of sodium ion must be responsible for the reduction in interfacial bond strength. Once moisture diffuses through the matrix and reaches the interface, it preferentially bonds to sodium and displaces the existing interfacial secondary bonds which provided the original interfacial adhesion.

Panex 33(S) fiber contained a considerable amount of residual sodium on the fiber surface. However, compared with AS-4-Na fiber, this system had a higher level of interfacial adhesion at both room temperature and elevated temperature humidity as shown in Figures 17 and 18. This result is again attributed to the surface roughness of this fiber. Under dry conditions, the secondary forces were stronger than the mechanical interlock contribution and dominated the interfacial bond strength. Under high humidity conditions, secondary force

Downloaded At: 11:17 22 January 2011

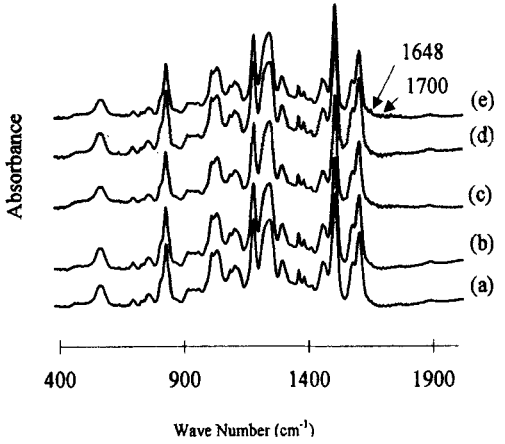

FIGURE 19 FTIR spectra of mPDA-cured Epon 828 epoxy resin. (a) original, (b) after 30 days in 23°C 100% RH, and (c) after 30 days in 23°C 10% Na_2CO_3 aqueous solution, (d) after 30 days in 75°C 100% RH, and (e) after 30 days in 75°C 10% Na_2CO_3 aqueous solution.

interactions were diminished by moisture interacting, while the relative contribution of mechanical interlocking increased.

G. Effect of Carbon Fiber Oxygen Plasma Treatment

The effect of fiber oxygen plasma treatment on the interfacial adhesion of AU-4 and Panex 33(U) fibers in Epon 828/mPDA matrix resin evaluated by interfacial shear strength measurement using the single-fiber fragmentation test are shown in Figures 20 and Figure 21. As a result of oxygen-plasma-induced surface changes, IFSS increased from about 30 and 31 to 52 and 60 MPa, respectively, for the AU-4 and Panex 33(U) fibers. The fiber surface oxygen/carbon ratio and polar surface energy are also plotted in Figures 20 and 21. Oxygen plasma treatment is more effective in increasing fiber surface oxygen content, surface energy, and fiber/matrix interfacial shear strength compared with commercial surface treatment (see Figs. 9 and 10 for comparison). The surface modification by plasma treatment was quite efficient, the steady state for measured properties being reached in about 15 seconds.

Downloaded At: 11:17 22 January 2011

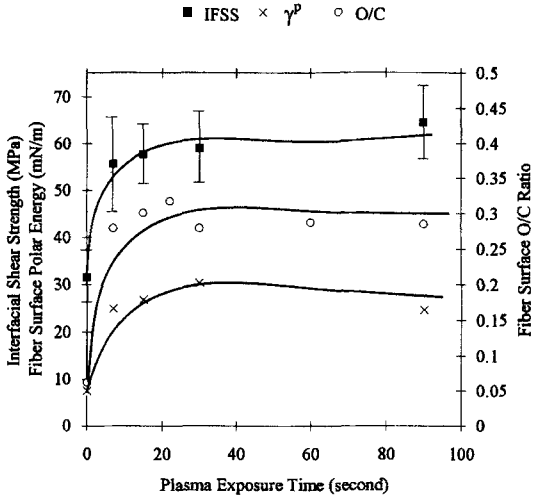

FIGURE 20 Interfacial shear strength as a function of oxygen plasma treatment time in AU-4 fiber and Epon 828/mPDA resin system.

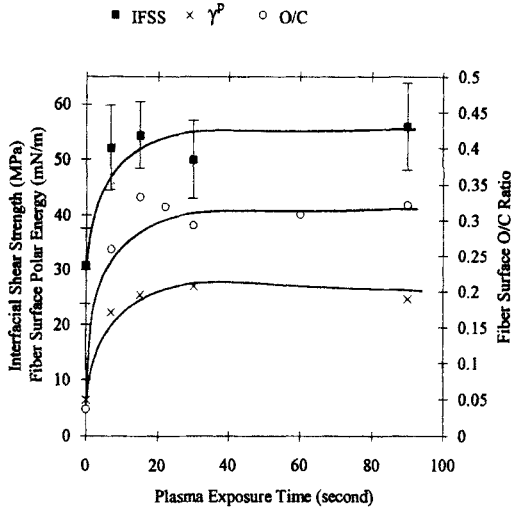

FIGURE 21 Interfacial shear strength as a function of oxygen plasma treatment time in Panex 33 (U) fiber and Epon 828/mPDA resin system.

IV. SUMMARY

Fiber surface topography examination by SEM showed that AU-4 and AS-4 fibers were essentially smooth and featureless, whereas Panex 33 fibers had a rather rough surface. The comparison of fibers before and after oxygen plasma treatment indicated that oxygen plasma resulted in etching and pitting of the AU-4 carbon fiber surface.

Carbon fiber surface XPS results revealed that commercially-surface-treated AS-4 and Panex 33(S) carbon fibers gave considerably higher surface oxygen atomic concentrations than those of untreated AU-4 and Panex 33(U) fibers. An even higher surface oxygen content was achieved by oxygen plasma treatment of AU-4 and Panex 33(U) fibers. A steady state oxygen content (about 20%) was reached in 15 seconds.

Compared with untreated fibers, commercial surface treated fibers had a higher surface energy predominantly in the polar part as measured by the two-liquid tensiometric test. The polar surface energy was increased even further for oxygen-plasma-treated fibers.

Fiber/matrix interfacial adhesion was evaluated using the single-fiber fragmentation test. Commercially-treated carbon fibers, which

Downloaded At: 11:17 22 January 2011

had higher surface oxygen contents and higher fiber surface energies, clearly produced higher interfacial shear strengths (IFSS), relative to untreated fibers. An even greater level of adhesion was achieved with oxygen-plasma-treated fibers.

Interfacial shear strength (IFSS) decreased with temperature in both the fiber/Epon 828-mPDA system where the test temperature was below the Tg of the matrix and the fiber/Epon 828-Jeffamine DU-700 system where the test temperature was above Tg. In the fiber/Epon 828-mPDA system, a quite dramatic decrease was observed at about 80°C which is considerably lower than the matrix Tg of 144°C. This decrease was attributed to the existence of a low Tg interphase region and the loss of secondary forces with increased temperature. Above 100°C, the IFSS of the commercial surface treated AS-4 fiber system dropped to the same level as that of the untreated AU-4 fiber system implying the higher IFSS of AS-4 compared with the AU-4 was essentially non-chemical in nature.

The IFSS of the fiber/Epon 828-mPDA system decreased when exposed to high humidity environments. The presence of surface sodium did not affect the initial interfacial adhesion. However, IFSS decreased dramatically when the fiber/matrix system was exposed to humidity. This phenomenon was attributed to the hygrometric property of sodium which led to water accumulation in the interface.

Fiber surface roughness did not enhance the initial interfacial adhesion strength. However, mechanical interlocking appeared to play a role when interfacial strength was lost by elevated humidity or elevated temperature.

Downloaded At: 11:17 22 January 2011

Acknowledgment

The authors sincerely acknowledge the financial support of this research by McDonnell Douglas Aerospace under agreement No. MDA972-93-2-0004. The technical assistance of Mr. Dale Fanter at Zoltek and Dr. James Craig, Mr. Frank Cromer, and Dr. Jack Lesko all at Virginia Tech is gratefully acknowledged.

References

[1] Harris, B., Beaumont, P. W. R. and de Ferran, E. M., *J. Mater. Sci.* **6**, 238 (1971).
[2] Drzal, L. T., in *Controlled Interphases in Composite Materials*, Ishida, H. (Elsevier Science, New York, 1990), p. 309.
[3] Cope, B. C., in *Handbook of Adhesion*, Packham, D. E., Ed. (Longman, Essex, 1992), p. 165.
[4] Donnet, J. B. and Bansal, R. C., in *Carbon Fibers*, 2nd ed. (Marcel Dekker, New York, 1990).
[5] McKee, D. W. and Mimeault, V. J., in *Chemistry and Physics of Carbon*, Vol. **8**, Walker, P. L., Jr., Ed. (Marcel Dekker, New York, 1973).
[6] Hammer, G. E. and Drzal, L. T., *Appl. Surf. Sci.* **4**, 340 (1980).
[7] Schultz, J., Cazeneuve, C., Shanahan, M. E. R. and Donnet, J. B., *J. Adhesion* **12**, 221 (1981).
[8] Owens, D. K. and Wendt, R. C., *J. Appl. Polym. Sci.* **13**, 1741 (1969).
[9] Fowkes, F. M., in *Treatise on Adhesion and Adhesives*, Vol. **1**, Patrick, R. L., Ed. (Marcel Dekker, New York, 1967), p. 352.
[10] Kelley, A. and Tyson, W. R. V., *J. Mech. Phys. Solids* **13**, 329 (1965).
[11] Drzal, L. T., Rich, M. J., Camping, J. D. and Park, W. J., *Proc. of 1980 Conf. of RP/Composites Inst., sec. 20-C*, 1980.
[12] Weibull, W., *J. Appl. Mech.* **18**, 293 (1951).
[13] Heisey, C. L., Ph.D., dissertation, Virginia Polytechnic Institute and State University, Blacksburg, Virginia, 1993.
[14] Beamson, G. and Briggs, D., in *High Resolution XPS of Organic Polymers* (John Wiley & Sons, New York, 1992).
[15] Desimoni, E., Casella, G. I., Morone, A. and Salvi, A. M., *Surf. Interf. Analysis* **15**, 627 (1990).
[16] Desimoni, E., Casella, G. I., Caladi, T. R. I., Salvi, A. M., Rotunno, T. and DiCroce, E., *Surf. Interf. Analysis* **18**, 623 (1992).
[17] Drzal, L. T., Rich, M. J. and Lloyd, P. F., *J. Adhesion* **16**, 1 (1982).
[18] Nardin, M., Asloun, E. M. and Schultz, J., *Composite Interf.* **1**(2), 113 (1993).
[19] Skourlis, T. P. and McCullough, R. L., *Composite Sci. Tech.* **49**, 363 (1993).
[20] Gerard, G. and Gilbert, A. C., *J. Appl. Mech. ASME* **24**, 355 (1957).
[21] Asloun, E. M., Nardin, M. and Schultz, J., *J. Mater. Sci.* **24**, 1835 (1989).
[22] Deiasi, R. and Whiteside, J. B., ASTM, STP 658 (ASTM, Philadelphia, 1978), p. 2.
[23] Drzal, L. T., Rich, M. J. and Koenig, M. F., *J. Adhesion* **18**, 49 (1985).
[24] Schutte, C. L., McDonough, W., Shioya, M., McAuliffe, M. and Greenwood, M., *Composites* **25**(7), 617 (1994).
[25] Kaelble, D. H. and Dynes, P. J., *J. Adhesion* **8**, 195 (1977).

Downloaded At: 11:17 22 January 2011